JVST A
Journal of Vacuum Science & Technology A

ARTICLE

pubs.aip.org/avs/jva

Low-resistivity molybdenum obtained by atomic layer deposition

Cite as: J. Vac. Sci. Technol. A **41**, 052402 (2023); doi: 10.1116/6.0002804
Submitted: 2 May 2023 · Accepted: 31 July 2023 ·
Published Online: 28 August 2023

Kees van der Zouw,[a] Bernhard Y. van der Wel, Antonius A. I. Aarnink, Rob A. M. Wolters, Dirk J. Gravesteijn, and Alexey Y. Kovalgin

AFFILIATIONS

MESA+ Institute for Nanotechnology, University of Twente, P.O. Box 217, Enschede 7500 AE, The Netherlands

Note: This paper is part of the 2024 Special Topic Collection on Atomic Layer Deposition (ALD).
[a]**Author to whom correspondence should be addressed:** k.vanderzouw@utwente.nl

ABSTRACT

A novel atomic layer deposition (ALD) process was developed for low-resistivity molybdenum (Mo) from molybdenum dichloride dioxide ($MoCl_2O_2$) and atomic hydrogen (at-H). A wide ALD window of self-limiting growth was observed between 150 and 450 °C. No film deposition occurred with molecular hydrogen (H_2), demonstrating the necessity to have at-H to efficiently reduce the $MoCl_2O_2$ precursor. At 350 °C and above, the film composition was determined at approximately 95 at. % of Mo and 3.5 at % of oxygen (O), with trace amounts (i.e., <1 at. %) of carbon (C), chlorine (Cl), hydrogen (H), and nitrogen (N). The growth per cycle (GPC) was roughly 0.022 nm/cycle. No substrate selectivity or pronounced nucleation delay was observed on silicon (Si), silicon dioxide (SiO_2), silicon nitride (Si_3N_4), silicon carbide (SiC), aluminum oxide (Al_2O_3), hafnium dioxide (HfO_2), and low-k dielectric (SiOC). Film uniformity and conformality were ±5% and ±10%, respectively, while resistivity approached a bulk value of 18.6 $\mu\Omega$ cm at 24 nm. At 250 °C and below, increased levels of oxygen (up to 33 at. % at 150 °C) and chlorine (2.7 at. % at 150 °C) were detected in the film. This trend coincided with an increase in the GPC, a change in optical properties, a decrease in film density and crystallinity, and an increase in resistivity. While self-limiting growth was observed through the entire ALD window of 150–450 °C, the temperature (T) range for depositing low-resistivity Mo deposition was narrower at $T \geq 250$ °C.

I. INTRODUCTION

The continuous miniaturization in the semiconductor industry is leading to new generations of chips with longer, narrower, and more closely packed interconnects. Interconnect speed has long been inconsequential, but increased RC delay and power consumption have rapidly become the major determinants of chip performance.[1–3] As critical interconnect dimensions reached below the electron mean free path (MFP)[4] of copper (Cu) and tungsten (W) in modern large-scale integrated circuits (ICs) and memories, enhanced electron scattering at surfaces and interfaces[5–8] greatly increased electrical resistivity of ultrathin interconnects.[9] Since both Cu and W possess a relatively long MFP, alternatives are being explored to replace copper as the interconnect in novel IC logic and tungsten as the word lines and contact material in 3D NAND memory devices.[10–14]

Solutions to reduce interconnect resistance can be found in novel device architectures, technologies, and materials.[3,15] The main candidates to replace copper and tungsten have been found among metals with low bulk resistivity and a short MFP. For example, ruthenium has been intensively investigated,[16–20] while cobalt has already been applied in commercial ICs.[21–24] Molybdenum (Mo) is seen as another potential candidate.[3,25–31] This refractory metal possesses a low coefficient of thermal expansion, high electrical conductivity and melting point, and relatively short MFP.[4] Its high thermal stability and expected resistance to electromigration could also alleviate the need for high-resistance diffusion barriers.[32–34] Mo metallization could, therefore, serve as a proxy for reliability and be considered an excellent alternative to replace Cu and W in advanced interconnects.

The introduction of new materials for interconnects is among the most difficult challenges in IC technology, mainly due to the stringent requirements for dimensional control, reliability, and processibility.[35] ALD has become a widely applied, mature technique

to realize materials for the semiconductor industry. Due to its attributes of sequential self-limiting surface reactions, ALD meets the requirements of precise thickness control, large-scale thickness uniformity, and conformality in high-aspect-ratio (HAR) structures.[36–38] However, a reliable ALD process for enabling metallic Mo films within the back-end-of-line (BEOL) limits is still missing.

Thin film deposition of pure Mo using ALD,[31,39,40] and, in particular, chemical vapor deposition (CVD),[41–60] has been studied extensively. Chemistries involving $MoCl_5$ reduction[41–45] or Mo $(CO)_6$ pyrolysis[46–50] or photolysis[51–55] generally require high process temperatures (>400 °C) to enable high-quality films. Processes based on MoF_6 reduction have been demonstrated below the BEOL temperature limit, but might suffer from corrosive byproducts (e.g., HF), precursor reduction by silicon, or undesired substrate selectivity.[56–60] ALD of Mo was performed by utilizing the reduction of Mo-oxychloride precursor by molecular hydrogen in the temperature range 450–590 °C.[31] Although film resistivity appeared to be promising, only a few experimental details were discussed. Furthermore, the temperature range was well beyond the BEOL limits. Recently, thermal ALD Mo was studied with $MoCl_2O_2$ as a precursor and H_2 as a coreactant in the temperature range of 600–650 °C.[61]

This work demonstrates the successful deposition of low-resistivity metallic molybdenum films from $MoCl_2O_2$ and atomic hydrogen (at-H) as the precursor and coreactant, respectively. Hot-wire (HW) assisted ALD (HWALD)[62] is utilized, in which at-H is produced by the dissociation of H_2 upon its interaction with a heated W filament. HWALD is considered an alternative to plasma-enhanced ALD to prevent potential plasma-induced damage.[63] In contrast to H_2, at-H allows for low-temperature reduction of $MoCl_2O_2$ in the temperature range of 150–450 °C.

II. EXPERIMENT

Molybdenum thin films were deposited in a home-built high vacuum hot-wall ALD reactor equipped with a low-volume reaction chamber. The reactor was pumped down to a base pressure of $\sim 1 \times 10^{-8}$ mbar using a turbomolecular pump. The vessel of the solid $MoCl_2O_2$ precursor (Air Liquide) was heated to 75 °C to ensure sufficient vapor pressure (~2 mbar) for the precursor to diffuse into the gas inlet (at 0.2 mbar overpressure). To prevent precursor condensation, the corresponding gas-inlet system and outside of the reactor were kept at 85 and 100 °C, respectively. Experiments were conducted with the reaction chamber heated to temperatures between 150 and 450 °C. The at-H was generated by feeding 20 SCCM of H_2 (Linde gas, 5.0) to a heated tungsten filament. The HW was shielded from the reaction chamber using a showerhead assembly, minimizing the influence of the HW on the substrate. The $MoCl_2O_2$ precursor and the at-H coreactant were introduced into the reaction chamber via separate gas inlets. A background pressure of $\sim 1 \times 10^{-3}$ mbar was obtained by applying 8 SCCM of N_2 carrier and purge gas (Linde gas, 5.0).

Mo thin films were deposited on Si(100), thermally grown SiO_2 and Si_3N_4, SiC, sapphire, ALD HfO_2 and a low-k industry-standard SiOC (k-value 3.0). The substrates were precleaned with either 99% HNO_3, 1% HF, or O_3 steam. There was no indication that film nucleation might be affected by the method of cleaning. The pulse durations used for a standard ALD cycle were 1 s of $MoCl_2O_2$ and 29 s of at-H, with both pulses separated from each other by 15 s N_2 purges. More details on the ALD cycle can be found in Sec. III. In addition to ALD, pulsed CVD experiments were conducted at conditions closely resembling those of the ALD process. Specifically, 1s $MoCl_2O_2$ pulses were introduced every 30 s under a constant at-H supply and without N_2 purges. This should ensure doses of $MoCl_2O_2$ and at-H comparable to those introduced in the ALD process.

Film growth was *in situ* monitored with a J. A. Woollam Co. M-2000 spectroscopic ellipsometer (SE) operating in the spectral range of 245–1690 nm. The growth per cycle (GPC) was determined by dividing the film thickness increase in the linear growth regime by the corresponding number of cycles. Additional SE measurements were performed *ex situ* with a J. A. Woollam Co. M-2000UI ellipsometer, equipped with an automatic goniometer, and sample alignment and positioning tools. The J. A. Woollam Co. CompleteEASE v6.46 software package was used to operate the SE and model the layer stack characteristics to extract the Mo thin film properties. The optical properties of Mo were modeled with a Drude term and two Lorentz oscillators. The former accounts for the intraband electron transitions, i.e., the existence of conduction electrons, while the latter describes interband transitions.[64] The accuracy of thickness determination for films thicker than 5 nm was verified through x-ray reflectometry (XRR) measurements and electron microscopy imaging. During *in situ* monitoring, both the optical characteristics and thickness of the Mo thin film were fitted by the SE software, to account for a possible variation in the optical properties with increasing film thickness. For films thinner than 5 nm, b-spline fitting was utilized to account for the potential appearance of new optical features.

XRR and grazing incidence x-ray diffraction (GIXRD) measurements were performed with a Rigaku SmartLab x-Ray diffractometer. The SmartLab Studio II software package was used to model the layer stack and to extract the Mo film thickness and density. The corresponding GPC was determined for XRR measurements by dividing the resulting film thickness by the total number of process cycles.

Mass spectroscopy analysis was performed with an MKS Spectra LM76 Microvision Plus quadrupole residual gas analyzer and Spectra Process Eye V2.0 software package.

Time-of-flight elastic recoil detection analysis (TOF-ERDA) of the elemental concentration profiles was performed with an EGP-10-II 5 MV tandem accelerator at the University of Helsinki. A 30 MeV 127I ion beam was used, with a recoil angle of 40° and 16° angle of incident relative to the sample surface. Elemental concentration depth profiles were calculated using SRIM-2003 stopping powers for energy loss calculations.

Secondary ion mass spectroscopy (SIMS) analysis was performed using an Atomika 4100 quadrupole SIMS tool. EAG proprietary software was used for quantification.

High-resolution scanning electron microscopy (SEM) images were obtained with a Zeiss Merlin HR-SEM by using an In-lens or energy-selective backscatter (ESB) detector. The In-lens detector allowed for clear topographic mapping, while the ESB detector was used for compositional contrast mapping. Scanning transmission

electron microscopy (STEM) images were captured with a Helios 5 Dual Beam from Thermo Fisher, while regular transmission electron microscopy (TEM) and energy-dispersive x-ray (EDX) spectroscopy images were obtained with an FEI cubed titan Cs-corrected 80–300 kV TEM.

Sheet resistance measurements were performed with a Polytec 280SI four-point probe station. Automatic custom cartesian wafer maps of 69 points with 1 cm intervals were obtained.

III. RESULTS AND DISCUSSION

A. ALD window determination

An appropriate ALD cycle was determined at 350 °C by evaluating the GPC with *in situ* SE, while independently varying the $MoCl_2O_2$ pulse time (t_1) and purge time (t_2), and the at-H pulse time (t_3) and purge time (t_4) durations. Being typical for ALD, the GPC stabilized with increasing t_1 and t_3, as depicted in Figs. 1(a) and 1(b), respectively. The GPC increased with decreasing t_2 [see Fig. 1(c)], presumably to an enhanced CVD contribution. Interestingly, the GPC was rather independent of the at-H purge time, as shown in Fig. 1(d). It supposedly indicated a very short at-H lifetime in the reactor; at-H might quickly recombine into H_2 and, thus, becomes nonreactive for both ALD and CVD modes. Based on Fig. 1, the standard ALD cycle was chosen as $\{t_1/t_2/t_3/t_4\} = \{1/15/29/15\}$ s, since it provided the near-saturation behavior of the GPC. A long at-H pulse time duration was chosen to ensure efficient reduction, as the extent of reduction may not be (fully) correlated with the magnitude of the GPC.

The necessity of using at-H, and not H_2, was confirmed by varying the hot-wire temperature [see Fig. 1(e)]. The GPC was first determined as a function of the HW power. The corresponding HW temperature was then estimated from our previous work with a similar HW setup.[65] The results clearly showed a quick decay in the GPC if the temperature of the HW was decreased, being attributed to the insufficient formation of at-H at lower filament temperatures. The growth stopped completely after the HW was turned off. Supplying only H_2 could not support film growth at the process conditions explored in this work.

The self-limiting nature of ALD was investigated over the temperature range between 150 and 450 °C through adsorption experiments, where $MoCl_2O_2$ was pulsed sequentially without pulsing

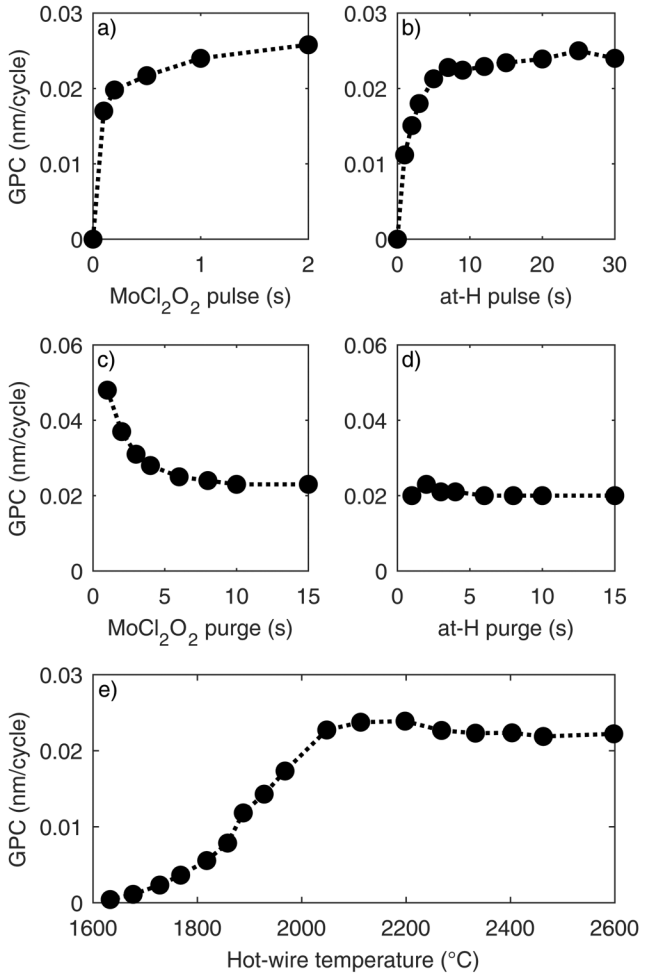

FIG. 1. GPC at 350 °C as a function of independently varied: (a) $MoCl_2O_2$ pulse time, (b) at-H pulse time, (c) $MoCl_2O_2$ purge time, (d) at-H purge time, and (e) hot-wire temperature.

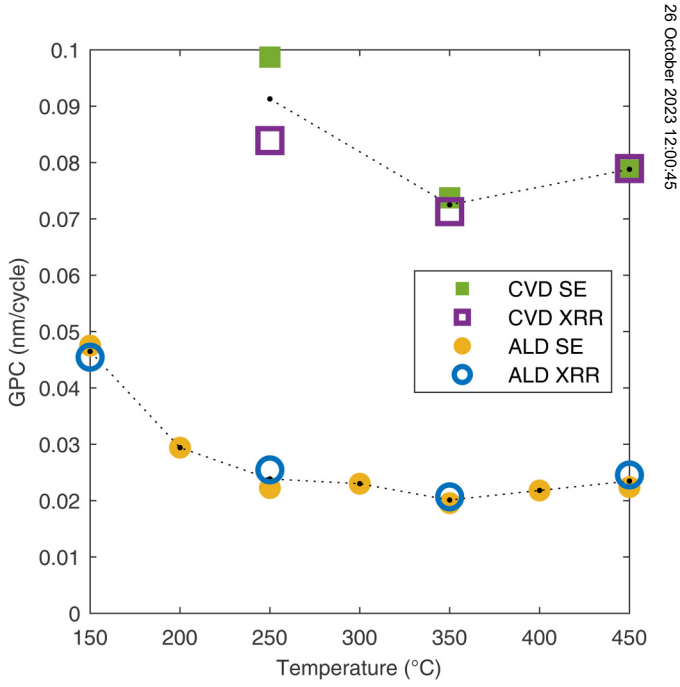

FIG. 2. GPC as a function of process temperature for both ALD (squares) and CVD (circles) experiments. SE measurements are indicated by open symbols, whereas XRR measurements are shown by solid symbols. The error bars are smaller than their respective markers.

at-H in between (see Fig. S1).[74] Saturation of the film thickness was observed for the entire temperature range, confirming the self-limiting nature of $MoCl_2O_2$ chemisorption.

The effect of substrate temperature (T_s) on the GPC was investigated for both ALD and pulsed CVD experiments, as shown in Fig. 2. Both *in situ* SE and *ex situ* XRR measurements, employed to determine the GPC, are in close agreement. The GPC slightly fluctuates around a constant value of ~0.022 nm/cycle for ALD ($250 \leq T_s \leq 450$ °C) and ~0.080 nm/cycle for CVD ($350 \leq T_s \leq 450$ °C). The difference in GPC between ALD and CVD modes suggests the presence of additional factors to enhance the GPC. This can be related to the occurrence of gas phase reactions and/or enhancement of surface reactions by the fact that both reactants are simultaneously present. Both ALD ($T_s < 250$ °C) and CVD ($T_s < 350$ °C) show an increase in GPC toward lowering T_s. The change in GPC in the low T_s range coincides with a change in the film optical properties from SE (see Fig. S2)[74] and a decrease in the film mass density according to XRR (see Fig. S3).[74] These observations can all be explained by an increased oxygen share in the films with lowering T_s, as further confirmed by elemental compositional analysis.

B. Deposition kinetics

Molybdenum layer growth kinetics was investigated by *in situ* SE, at different temperatures ($T_s = 150$–450 °C, only on Si) and on various substrates (at $T_s = 350$ °C only). Thin films were successfully deposited on Si, SiO_2, Si_3N_4, SiC, HfO_2, Al_2O_3, and low-k SiOC. Figure 3 shows the thickness evolution of Mo on SiO_2 for the first 400 ALD cycles. One should bear in mind that not solely the thickness but also the optical properties are fitting parameters in the SE model, because of their expected dependence on the film thickness. From Fig. 3, the initial nucleation stage is followed by a linear thickness increase, demonstrating a constant GPC. The onset of the steady growth regime is estimated at approximately 3–3.5 nm of the film thickness. Unfortunately, no conclusive statement can be made about the nature of film growth (substrate inhibited or enhanced) in the nucleation stage. The SE-determined thickness was verified by other measurement techniques (e.g., XRR, SEM, and TEM) for values exceeding 5 nm but not below 5 nm. A substrate-inhibited type of growth may be expected when considering the evolution of the GPC with the number of cycles, as depicted in the inset of Fig. 3, where the GPC increases rapidly, approaches a maximum, and finally, decreases to a steady value.[66] However, if the film thickness is extrapolated from the stable growth regime to zero cycles, the curve would intersect the positive y axis, which would only be possible for growth that is enhanced in the incubation regime. Nevertheless, no pronounced nucleation delay was observed for any of the substrates and temperatures investigated, as can be seen in Fig. S4.[74]

Mass spectroscopy (MS) was used to investigate the evolution of byproducts during the chemisorption of $MoCl_2O_2$ and its subsequent reaction with at-H, as depicted in Fig. 4. MS was employed outside of the standard ALD process conditions in order to prevent a sensor overload. Introducing a saturation $MoCl_2O_2$ pulse of 1s to a substrate pre-exposed to at-H is accompanied by a significant elimination of HCl and only a little H_2O. Oppositely, a subsequent

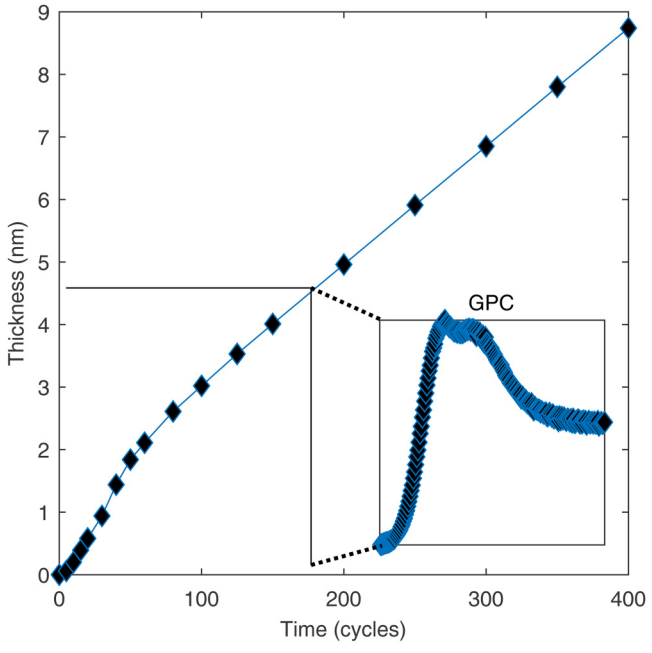

FIG. 3. Thickness of the Mo film as a function of time during the initial stages of the ALD process. Inset: GPC in the incubation regime.

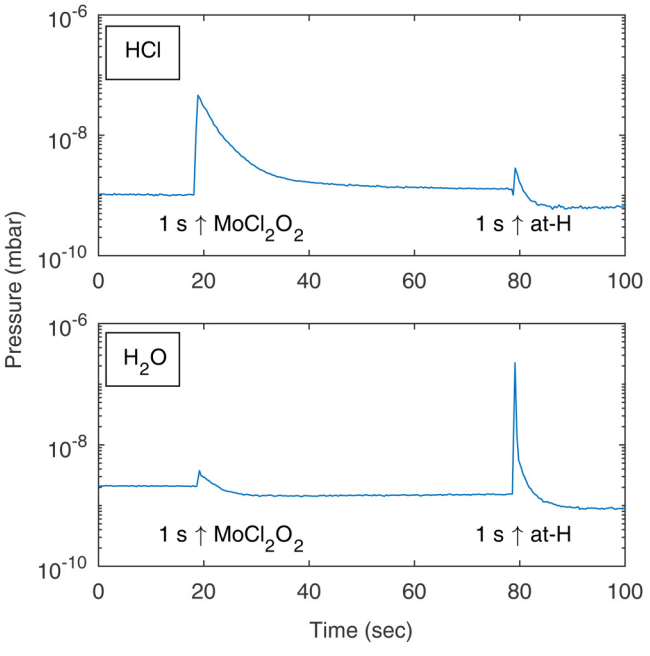

FIG. 4. Evolution of HCl and H_2O byproduct emission for the $MoCl_2O_2$ + at-H ALD process, as determined by mass spectroscopy.

at-H pulse of 1s coincides with considerable H_2O elimination and only a weak HCl production. These results suggest that the initial $MoCl_2O_2$ chemisorption occur primarily through the interaction between surface hydrogen and precursor chloride ligands, forming HCl. At-H is expected to further remove most of the O and remaining Cl ligands through the formation of H_2O and HCl, respectively.

C. Compositional analysis

The film composition was investigated by time-of-flight elastic recoil detection analysis (TOF-ERDA). Figure 5(a) depicts the TOF-ERDA depth profile of Mo, O, and Si in a 20 nm thick ALD film obtained at 350 °C on a Si substrate. (To be noted: other elements such as Cl, H, C, and N are only present in trace amounts, i.e., below 1 at. %.) The two oxygen peaks correspond to the surface oxides: the surface MoO_x and interfacial native SiO_2, respectively. The temperature dependence of the elemental composition is shown in Fig. 5(b), including the common contaminants. For $T_s \geq 350$ °C, the films roughly consist of 95 at. % of Mo and 3.5 at. % of O. Trace amounts of H, C, and N are measured at 0.7, 0.2, and 0.3 at. %, respectively. The share of Cl is below the detection limit. Importantly, the oxygen share shows an increase toward lower temperatures, being 6.6 at. % at 250 °C and 33.3 at. % at 150 °C. Furthermore, the share of chlorine becomes non-negligible at 2.7 at. % at 150 °C. These results may indeed indicate that the (i) increase in the GPC, (ii) decrease in the film density, and (iii) variation in the film optical properties, all observed with lowering T_s, can be explained by the change in film composition due to the increasing inability of at-H to efficiently remove the ligands from the $MoCl_2O_2$ precursor.

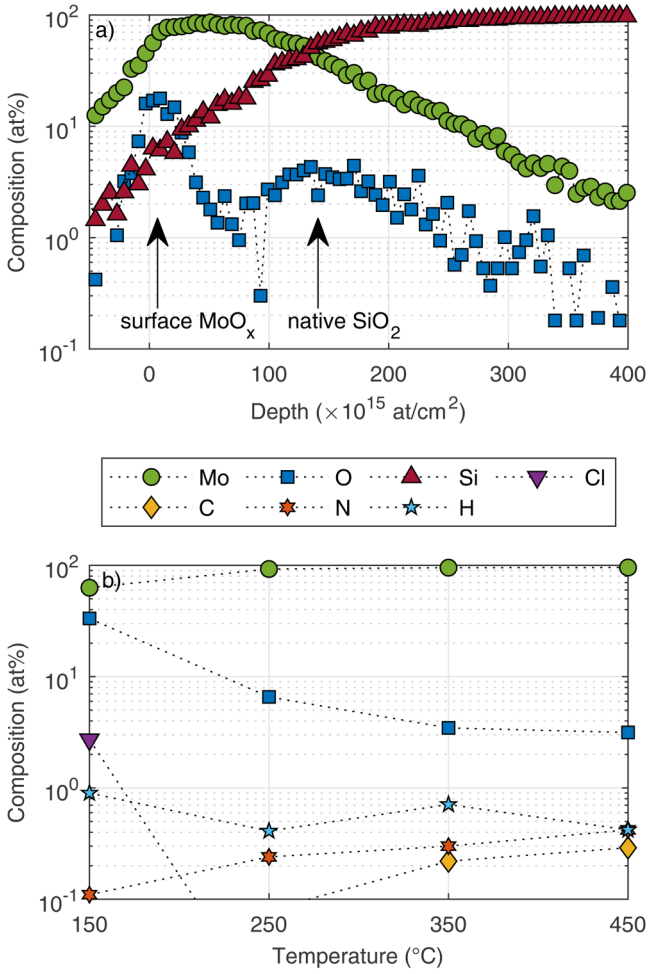

FIG. 5. TOF-ERDA measurements showing (a) a compositional depth profile of an ALD film obtained at 350 °C and (b) averaged ALD film composition at various temperatures.

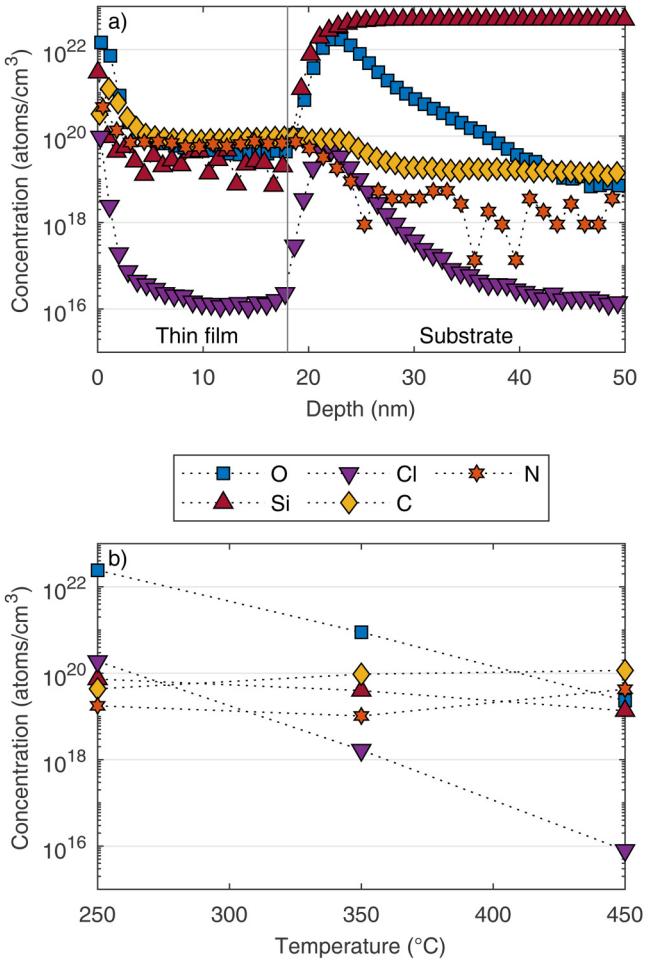

FIG. 6. SIMS measurements with (a) a concentration depth profile of the elements in a Mo ALD film obtained at 350 °C and (b) elemental concentrations in CVD films deposited at various temperatures.

Secondary ion mass spectrometry (SIMS) depth profiles were obtained to further investigate the elemental composition. From the depth profile of an ALD film obtained at 350 °C on a Si substrate, as shown in Fig. 6(a), it can be seen that O, Cl, C, N, and Si contaminants are only present in trace amounts of around 10^{20} atoms/cm^3. The CVD-SIMS results [see Fig. 6(b)] show an increase in the O and Cl shares toward lower temperatures. While the amount of Cl only approaches 10^{20} atoms/cm^3, the amount of oxygen exceeds 10^{22} atoms/cm^3 for a CVD film grown at 250 °C. This is expected to correspond to a few tens of atomic percent of oxygen in this film, once again confirming the compositional changes and corresponding properties at such a low temperature.

D. Film resistivity

The electrical resistivity of Mo was determined by four-point probe sheet resistance measurements and SE thickness determination. Figure 7(a) shows resistivity as a function of film thickness. The resistivity approaches a bulk value of 18.6 $\mu\Omega$ cm for an approximately 24 nm thick ALD film deposited at 350 °C on SiO_2. The resistivity of Mo films obtained in the other ALD works was 13 $\mu\Omega$ cm (at 600–650 °C),[61] 15 $\mu\Omega$ cm (at 400–500 °C),[39] 16 $\mu\Omega$ cm (at 450–590 °C),[31] and 124 $\mu\Omega$ cm (at 120 °C).[40] In this work, the temperature did not exceed 350 °C. The as-obtained resistivity of 18.6 $\mu\Omega$ cm was thus considered to be sufficiently low and in line with the reported dependence of resistivity on the film deposition temperature. The resistivity starts to increase sharply with decreasing film thickness if the film thickness approaches the electron MFP in molybdenum (at 11.2 nm).[4] Figure 7(b) shows resistivity as a function of process temperature, both for ALD and CVD films on Si with native SiO_2. All films are approximately 25 nm thick, except for the ALD film deposited at 150 °C, whose lower density resulted in a film thickness that approached 50 nm. A correction to the resistivity has been applied to account for the parallel conduction path through the Si substrate.[67] As expected, the resistivity is low for deposition at higher temperatures, while it increases sharply with decreasing temperatures below 250 °C for ALD and below 350 °C for CVD. These trends are in agreement with the trends observed for oxygen incorporation (Figs. 5 and 6). The increase in film resistivity at lower temperatures can also originate from a loss of crystallinity. As shown in Fig. 8, a GIXRD measurement of the ALD film obtained at 350 °C reveals peaks at 41°, 59°, and 74°, which corresponds to the (110), (200), and (211) planes of BCC Mo, respectively.[31,61] In contrast, besides a peak from the (311) plane of the p-Si(100) substrate,[68,69] no peaks are observed for the ALD sample obtained at 150 °C, which indicates an amorphous nature of the film.

E. Film uniformity and conformality

Film thickness and sheet resistance were further mapped across the wafer surface (see Figs. S5 and S6).[74] The results showed good uniformity with a circle of ~7 cm in diameter, centered on a 100 mm wafer, with ±5% variations. The nonuniformity radially increased toward the wafer edge. Since at-H entered the reactor above the center of the wafer, the observed nonuniformity

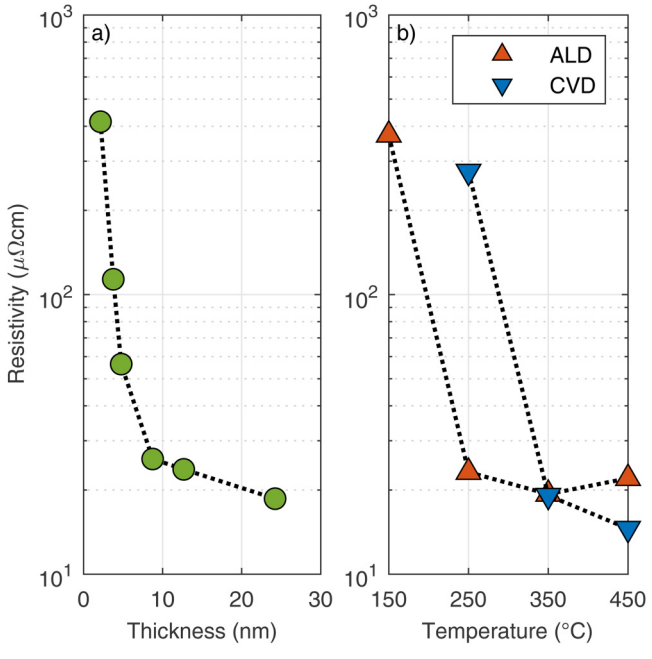

FIG. 7. Film resistivity as a function of (a) the ALD film thickness and (b) process temperature.

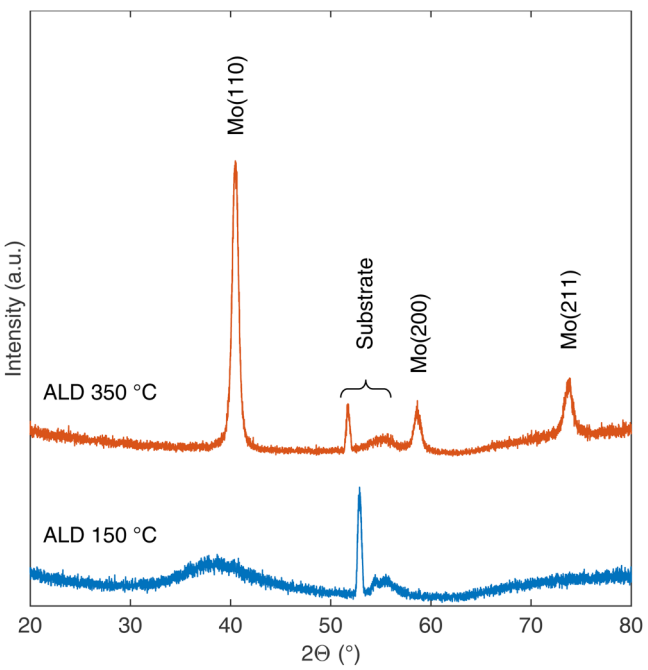

FIG. 8. GIXRD patterns of the ALD Mo films deposited at 150 and 350 °C.

confirmed once more the crucial role of at-H in the film formation process. The purge time experiments shown in Fig. 1 already suggested the residence time of at-H in the reactor to be rather short. The observed nonuniformity might suggest a limited delivery of at-H to the wafer edge, limiting process chemistry.

Film conformality was investigated in HAR trenches (the aspect ratio varying between 2:1 and 10:1) by scanning TEM, as shown in Fig. 9(a). The Si trenches had a SiO_2 capping, on which Mo was deposited. Film conformality, defined as the film thickness at a particular position in the trench divided by that on top of the trench, is estimated at 95% on the sidewalls and 90% at the bottom of the 3:1 trench. The conformality decreases with narrowing the trenches (i.e., increasing the aspect ratio), presumably due to increased hydrogen recombination and reduced reactant as well as byproduct diffusion into/out of the trenches.[70–72]

Fast Fourier transform (FFT) analysis of the TEM images [see Fig. 9(b)] reveals rings with d spacings of 2.22, 1.57, and 1.26 Å, corresponding to the body-centered cubic (BCC) structure of molybdenum.[73] Figures 10(a), 10(c), and 10(e) show a STEM image and elemental mapping of molybdenum and oxygen atoms (EDX measurements) near the top surface of a narrow trench, revealing their uniform distribution. From Figs. 10(b), 10(d), and 10(f), it is evident that the Mo precursor is able to diffuse all the way down to the bottom of the trench. However, from an EDX line integral, it follows that the share of oxygen is increased by roughly a factor of 2, pointing to possible limitations for the diffusion of at-H in narrow trenches. Possibly, at-H recombined by collisions with the walls. The chlorine shares are low and reasonably uniform from top to bottom. The results indicate that the formation of pure Mo in HAR structures may require giving longer pulses of at-H, to ensure its sufficient concentration at the bottom of the trench.

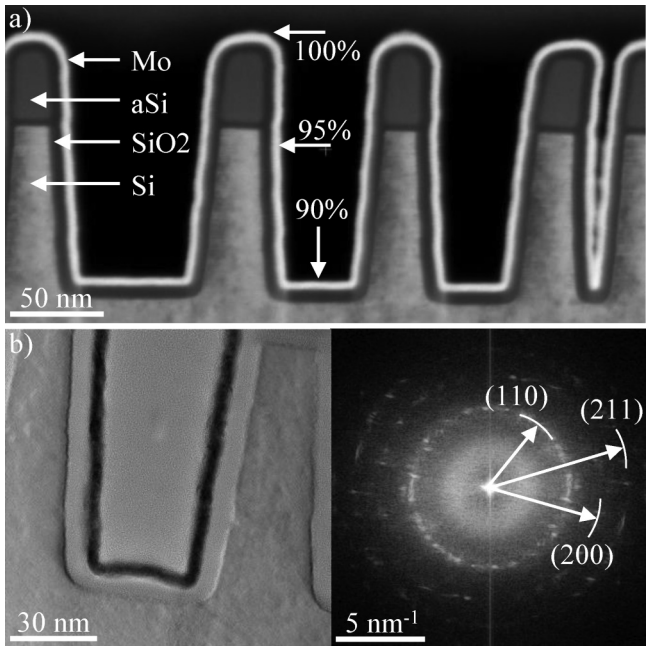

FIG. 9. TEM analysis with (a) STEM image of the layer stack and conformality estimate and (b) TEM image and FFT analysis.

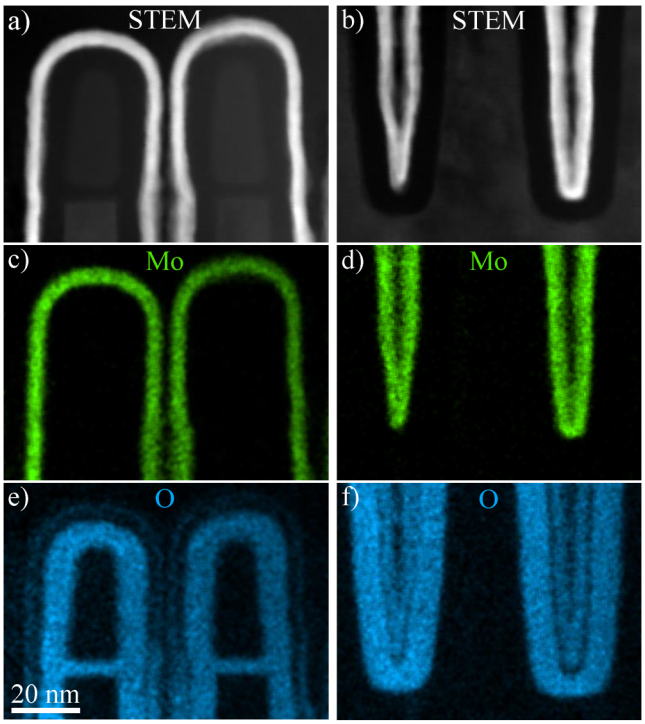

FIG. 10. EDX analysis, with STEM [(a) and (b)], molybdenum [(c) and (d)], and oxygen [(e) and (f)] elemental mapping, for the top [(a), (c), and (e)] and the bottom [(b), (d), and (f)] of a narrow trench.

IV. SUMMARY AND CONCLUSIONS

A novel hot-wire-assisted ALD process was developed for enabling low-resistivity Mo films from $MoCl_2O_2$ and at-H. Self-limiting growth was observed in the temperature range between 150 and 450 °C. Pulsing molecular hydrogen instead of at-H did not reveal any deposition of Mo. The ALD process was compared with the CVD process under similar conditions. The GPC in the ALD window exhibited a value of approx. 0.022 or 0.080 nm/cycle for ALD or CVD, respectively. The GPC increased with lowering the temperature below 250 °C for ALD and below 350 °C for CVD, which was attributed to the incomplete precursor reduction giving higher oxygen and chlorine shares in the films. The best elemental composition by TOF-ERDA revealed approximately 95 at. % of Mo, 3.5 at. % of O, and trace amounts (i.e., <1 at. %) of C, Cl, H, and N. This demonstrated the ability of at-H to efficiently reduce the $MoCl_2O_2$ precursor. Lowering deposition temperature led to the change of optical film constants, decreased film mass density, higher O and Cl shares, and subsequently, increased electrical resistivity of the films, suggesting the formation of Mo suboxides. The experiments showed the capability to deposit

Mo films on different substrates (Si, SiO_2, Si_3N_4, SiC, Al_2O_3, HfO_2, and low-k SiOC) and in a wide temperature range (150–450 °C) without any pronounced nucleation delay. The electrical film resistivity was measured at 18.6 $\mu\Omega$ cm for approximately 24 nm thick ALD films and increased sharply for thicknesses below the intrinsic electron MFP in Mo. Film uniformity and conformality in HAR structures were satisfactory, with ±5% and ±10% variations, respectively. Mo could be deposited in narrow trenches but with increased oxygen shares.

ACKNOWLEDGMENTS

This work has been financially supported by the Topconsortium for Knowledge and Innovation (TKI) funds of The Netherlands and ASM. The authors thank Y. Bu, M. J. Goodwin, and M. A. Smithers of the MESA+ Institute for XPS, FIB, and HR-SEM analysis, respectively. We had the pleasure of working with S. D. Dulfer, who performed four-point probe electrical resistance measurements. F. D. Tichelaar of TU Delft is acknowledged for his TEM analysis.

AUTHOR DECLARATIONS

Conflict of Interest

The authors have no conflicts to disclose.

Author Contributions

Kees van der Zouw: Formal analysis (lead); Investigation (lead); Visualization (lead); Writing – original draft (lead); Writing – review & editing (lead). **Bernhard Y. van der Wel:** Formal analysis (supporting); Investigation (supporting); Visualization (supporting); Writing – review & editing (supporting). **Antonius A. I. Aarnink:** Investigation (supporting); Supervision (supporting); Writing – review & editing (supporting). **Rob A. M. Wolters:** Supervision (supporting); Writing – review & editing (supporting). **Dirk J. Gravesteijn:** Supervision (supporting); Writing – review & editing (equal). **Alexey Y. Kovalgin:** Project administration (lead); Supervision (lead); Writing – review & editing (lead).

DATA AVAILABILITY

The data that support the findings of this study are available from the corresponding author upon request.

REFERENCES

[1]P. Kapur, J. P. McVittie, and K. C. Saraswat, IEEE Trans. Electron Devices **49**, 590 (2002).
[2]M. R. Baklanov, C. Adelmann, L. Zhao, and S. De Gendt, ECS J. Solid State Sci. **4**, Y1 (2015).
[3]Zs. Tőkei *et al.*, in *International Electron Devices Meeting* San Francisco, CA, 12-18 December 2020 (IEEE, New York, 2020), pp. 5.3.1–5.3.4.
[4]D. Gall, J. Appl. Phys. **119**, 085101 (2016).
[5]K. Fuchs, Math. Proc. Camb. Philos. Soc. **34**, 100 (1938).
[6]E. H. Sondheimer, Adv. Phys. **1**, 1 (1952).
[7]A. F. Mayadas, M. Shatzkes, and J. F. Janak, Appl. Phys. Lett. **14**, 345 (1969).
[8]A. F. Mayadas and M. Shatzkes, Phys. Rev. B **1**, 1382 (1970).
[9]D. Josell, S. H. Brongersma, and Z. Tőkei, Annu. Rev. Mater. Res. **39**, 231 (2009).
[10]C. Adelmann *et al.*, in *IEEE IITC* San Jose, CA, 20-23 May 2014 (IEEE, New York, 2014), pp. 173–176.
[11]K. Sankaran, S. Clima, M. Mees, and G. Pourtois, ECS J. Solid State Sci. **4**, N3127 (2015).
[12]C. Adelmann *et al.*, in *IEEE IITC* Santa Clara, CA, 4-7 June 2018 (IEEE, New York, 2018), pp. 154–156.
[13]D. Gall, in *International Symposium on VLSI Technology Systems* Hsinchu, Taiwan, 10-13 August 2020 (IEEE, New York, 2020), pp. 112–113.
[14]D. Gall, J. Appl. Phys. **127**, 050901 (2020).
[15]A. S. Oates, in *International Symposium on VLSI Design, Automation, and Testing* Hsinchu, Taiwan, 28-30 April 2014 (IEEE, New York, 2014), p. 1.
[16]L. G. Wen *et al.*, ACS Appl. Mater. Interfaces **8**, 26119 (2016).
[17]L. G. Wen *et al.*, in *IEEE IITC/AMC* San Jose, CA, 23-26 May 2016 (IEEE, New York, 2016), pp. 34–36.
[18]S. Dutta, S. Kundu, A. Gupta, G. Jamieson, J. F. Gomez Granados, J. Bömmels, C. J. Wilson, Z. Tőkei, and C. Adelmann, IEEE Electron Device Lett. **38**, 949 (2017).
[19]S. Dutta, K. Moors, M. Vandemaele, and C. Adelmann, IEEE Electron Device Lett. **39**, 268 (2018).
[20]D. Wan *et al.*, in *IEEE IITC* Santa Clara, CA, 4-7 June 2018 (IEEE, New York, 2018), pp. 10–12.
[21]J. Kelly *et al.*, in *IEEE IITC/AMC* San Jose, CA, 23-26 May 2016 (IEEE, New York, 2016), pp. 40–42.
[22]S. Dutta *et al.*, IEEE Electron Device Lett. **39**, 731 (2018).
[23]C. Auth *et al.*, in *International Electron Devices Meeting* San Francisco, CA, 2-6 December 2017 (IEEE, New York, 2017), pp. 29.1.1–-29.1.4.
[24]F. Griggio *et al.*, Int. Rel. Phys., Burlingame, CA, 11-15 March 2018 (IEEE, New York, 2018).
[25]A. Gupta *et al.*, in *International Electron Devices Meeting* San Francisco, CA, 11-16 December 2021 (IEEE, New York, 2021), pp. 22.5.1–22.5.4.
[26]V. Founta *et al.*, Materialia **24**, 101511 (2022).
[27]A. Ajaykumar *et al.*, in *S. VLSI Technology* Kyoto, Japan, 13-19 June 2021 (IEEE, New York, 2021), pp. 1–2.
[28]H. Kösterbauer, H. Schmidt, D. Lorenz, C. Linke, Y. Zhang, C. Dong, and J. Winkler, SID Symp. Dig. Tech. Pap. **51**, 200 (2020).
[29]P. Kreiml, M. Rausch, V. L. Terziyska, H. Köstenbauer, J. Winkler, C. Mitterer, and M. J. Cordill, Thin Solid Films **665**, 131 (2018).
[30]D. Tierno, M. Hosseini, M. van der Veen, A. Dangol, K. Croes, S. Demuynck, Zs. Tőkei, E. D. Litta, and N. Horiguchi, in *IEEE IITC* Kyoto, Japan, 6-9 July 2021 (IEEE, New York, 2021), p. 1.
[31]E. Zoubenko, S. Iacopetti, K. Weinfeld, Y. Kauffmann, P. Van Cleemput, and M. Eizenberg, J. Vac. Sci. Technol. A **39**, 043201 (2021).
[32]C. S. Hau-Riege, Microelectron. Reliab. **44**, 195 (2004).
[33]A. S. Oates, ECS J. Solid State Sci. **4**, N3168 (2015).
[34]K. Croes *et al.*, in *IEEE International Electron Devices Meeting* San Francisco, CA, 1-5 December 2018 (IEEE, New York, 2018), pp. 5.3.1–5.3.4.
[35]IEEE International Roadmap for Devices and Systems (2022), available at https://irds.ieee.org.
[36]R. L. Puurunen, Chem. Vap. Deposition **9**, 249 (2003).
[37]S. M. George, Chem. Rev. **110**, 111 (2010).
[38]V. Cremers, R. L. Puurunen, and J. Dendooven, Appl. Phys. Rev. **6**, 021302 (2019).
[39]M. Juppo, M. Vehkamäki, M. Ritala, and M. Leskelä, J. Vac. Sci. Technol. A **16**, 2845 (1998).
[40]D. Seghete, G. B. Rayner, Jr., A. S. Cavanagh, V. R. Anderson, and S. M. George, Chem. Mater. **23**, 1668 (2011).
[41]W. J. Childs, J. E. Cline, W. M. Kisner, and J. Wulff, Trans. Am. Soc. Metal. **43**, 105 (1951).
[42]J. J. Casey, R. R. Verderber, and R. R. Garnache, J. Electrochem. Soc. **114**, 201 (1967).
[43]T. Sugano, H.-K. Chou, M. Yoshida, and T. Nishi, Jpn. J. Appl. Phys. **7**, 1028 (1968).
[44]G. E. Carver, D. D. Allred, and B. O. Seraphin, Proc. SPIE **0161**, 66 (1978).

[45]C. Duty, R. Johnson, S. Bondi, and W. J. Lackey, Chem. Vap. Deposition **9**, 298 (2003).
[46]L. H. Kaplan and F. M. d'Heurle, J. Electrochem. Soc. **117**, 693 (1970).
[47]A. I. DeRosa, D. B. Dove, and R. E. Loehman, J. Vac. Sci. Technol. **11**, 455 (1974).
[48]G. E. Carver, Solar Energy Mater. **1**, 357 (1979).
[49]Z. Song, T. Cai, J. A. Rodriguez, J. Hrbek, A. S. Y. Chan, and C. M. Friend, J. Phys. Chem. B **107**, 1036 (2003).
[50]E. Mohimi, Z. V. Zhang, S. Liu, J. L. Mallek, G. S. Girolami, and J. R. Abelson, J. Vac. Sci. Technol. A **36**, 041507 (2018).
[51]R. Solanki, P. K. Boyer, and G. J. Collins, Appl. Phys. Lett. **41**, 1048 (1982).
[52]D. K. Flynn, J. I. Steinfeld, and D. S. Sethi, J. Appl. Phys. **59**, 3914 (1986).
[53]H. H. Gilgen, T. Cacouris, P. S. Shaw, R. R. Krchnavek, and R. M. Osgood, Appl. Phys. B **42**, 55 (1987).
[54]G. A. Kovall, J. C. Matthews, and R. Solanki, J. Vac. Sci. Technol. A **6**, 2353 (1988).
[55]C. C. Cho and S. L. Bernasek, J. Appl. Phys. **65**, 3035 (1989).
[56]S. H. Smiley, D. C. Brater, and H. L. Kaufman, J. Mater. **17**, 605 (1965).
[57]J. G. Donaldson and H. Kenworthy, Electrodepos. Surf. Treat. **2**, 435 (1974).
[58]N. Lifshitz, D. S. Williams, C. D. Capio, and J. M. Brown, J. Electrochem. Soc. **134**, 2061 (1987).
[59]A. Hårsta and J.-O. Carlsson, Thin Solid Films **185**, 235 (1990).
[60]K. L. Björklund, P. Heszler, and M. Boman, Appl. Surf. Sci. **186**, 179 (2002).
[61]B.-J. Lee, K.-B. Lee, M.-H. Cheon, D.-W. Seo, and J.-W. Choi, Coatings **13**, 1070 (2023).
[62]A. Y. Kovalgin, M. Yang, S. Banerjee, R. O. Apaydin, A. A. I. Aarnink, S. Kinge, and R. A. M. Wolters, Adv. Mater. Interfaces **4**, 1700058 (2017).
[63]H. B. Profijt, S. E. Potts, M. C. M. van de Sanden, and W. M. M. Kessels, J. Vac. Sci. Technol. A **29**, 050801 (2011).
[64]H. Fujiwara, *Spectroscopic Ellipsometry: Principles and Applications* (Wiley, New York, 2007).
[65]A. J. Onnink, J. Schmitz, and A. Y. Kovalgin, Thin Solid Films **674**, 22 (2019).
[66]R. L. Puurunen and W. Vandervorst, J. Appl. Phys. **96**, 7686 (2004).
[67]Y.-Y. Chen and J.-Y. Juang, Meas. Sci. Technol. **27**, 074006 (2016).
[68]B.-O. Cho, J. P. Chang, J.-H. Min, S. H. Moon, Y. W. Kim, and I. Levin, J. Appl. Phys. **93**, 745 (2003).
[69]L. Y. Zhao, H. Jalili, N. Panjwani, T. Chan, Z. H. He, N. F. Heinig, and K. T. Leung, Electrochem. Solid-State Lett. **10**, K47 (2007).
[70]J. Dendooven, D. Deduytsche, J. Musschoot, R. L. Vanmeirhaeghe, and C. Detavernier, J. Electrochem. Soc. **156**, P63 (2009).
[71]J. Dendooven, D. Deduytsche, J. Musschoot, R. L. Vanmeirhaeghe, and C. Detavernier, J. Electrochem. Soc. **157**, G111 (2010).
[72]H. C. M. Knoops, E. Langereis, M. C. M. van de Sanden, and W. M. M. Kessels, J. Electrochem. Soc. **157**, G241 (2010).
[73]D. R. Lide, *CRC Handbook of Chemistry and Physics* (CRC Press, Boca Raton, Florida, 2003).
[74]See the supplementary material online for additional metrology of the Mo ALD process development.